Bayesian inference of the crust-core transition density via the neutron-star radius and neutron-skin thickness data

Wen-Jie Xie* Zi-Wei Ma, Jun-Hua Guo
[1]*Department of Physics, Yuncheng University, Yuncheng 044000, China*
(Dated: March 23, 2023)

In this work we perform a Bayesian inference of the crust-core transition density ρ_t of neutron stars based upon the neutron-star radius and the neutron-skin thickness data within a thermodynamical method. The uniform and Gaussian distributions for the ρ_t prior are adopted in the Bayesian approach. It has a larger probability to have values higher than 0.1 fm^{-3} for ρ_t as the uniform prior and the neutron-star radius data are used. We found that this is controlled by the curvature $K_{\rm sym}$ of the nuclear symmetry energy. This phenomenon will not happen if $K_{\rm sym}$ is not extremely negative, i.e., $K_{\rm sym}$ > -200 MeV. The obtained ρ_t is $0.075^{+0.005}_{-0.01}$ fm^{-3} at 68% confidence level when both the neutron-star radius and the neutron-skin thickness data are taken into account. The strongly anti-correlations between ρ_t and the slope L, curvature of the nuclear symmetry energy are observed. The dependence of the three L-$K_{\rm sym}$ correlations predicted in the literature on the crust-core density and pressure is quantitatively investigated. The most probable value of 0.08 fm^{-3} for ρ_t is obtained from the L-$K_{\rm sym}$ relation raised by Holt *et al.* and the larger values are preferred by the other two relations.

PACS numbers:

Keywords: Crust-core transition density of neutron stars, Neutron-star radius, Neutron-skin thickness, Bayesian inference approach, L-$K_{\rm sym}$ correlations

I. INTRODUCTION

The determination of the crust-core transition density ρ_t in neutron stars (NSs) is important for not only the predictions of the bulk NS properties[1] but also the finite nuclei properties[2–4]. However, due to the intricate structure of the inner crust in NSs, constraining the transition density is still challenging. Various theoretical models have been used to estimate the transition density in the past years including the dynamical method[5–9], the Thomas-Fermi approximation method[10], the random phase approximation[4], the thermodynamical method[11–13], the Vlasov method[14], the compressible liquid-drop model[15] and the meta-modeling approach[16]. These methods give different predictions, i.e., ρ_t=0.071±0.011 fm^{-3} estimated in the meta-modeling approach[16], ρ_t=0.0955±0.0007 fm^{-3} obtained by comparing with the excitation energies of giant resonances, energy-weighted pygmy dipole strength, and dipole polarizability data using the relativistic nuclear energy density functionals[2], ρ_t=0.04∼0.065 fm^{-3} limited by using the EOS including the momentum-dependent interaction of neutron-rich nuclear matter constrained by the isospin diffusion data in heavy-ion reactions[8], ρ_t=0.069∼0.098 fm^{-3} from the thermodynamical method[13] and ρ_t=0.058∼0.092 fm^{-3} with the Thomas-Fermi method[10] and so on. These predicted by the dynamical method are usually smaller than that from the thermodynamical method by about 0.01 fm^{-3}[8].

The nuclear symmetry energy plays a dominant role in accurately describing the crust-core interface of NSs. It has been known that the crust-core transition density is highly sensitive to the isospin dependence of the nuclear equation of state (EOS)[1]. Especially, the slope L and curvature $K_{\rm sym}$ of the nuclear symmetry energy as well as the L-$K_{\rm sym}$ correlation have been reported to be strongly correlated with the crust-core transition density[12, 15, 16]. In a recent work[15], a Bayesian approach is used to infer the distribution of ρ_t based on the low density constraints for neutron and symmetric nuclear matter from the effective field theory. However, the obtained ρ_t distribution and the correlations between ρ_t and the EOS parameters highly depend on the surface energy parameter. In the present work, we perform a Bayesian inference of the crust-core transition density in NSs based on the NS radius and neutron-skin thickness data. The dependence of the L-$K_{\rm sym}$ correlations predicted in the literature on the posterior distributions of ρ_t are discussed.

The rest of paper is organized as follows. In the next section, we outline the theoretical framework including the thermodynamical method, the EOS meta-modeling method, the nuclear droplet model and the Bayesian inference approach. In the section III, we probe the crust-core transition density and its correlations with the EOS parameters via the NS radius and neutron-skin thickness data in the Bayesian framework. We also explore the effect of the L-$K_{\rm sym}$ correlation on the crust-core transition density and pressure. A summary is given at the end.

*Corresponding author: wenjiexie@yeah.net

II. THEORETICAL FRAMEWORK

A. Crust-core transition density and isospin-dependent parametric EOS for the core of NSs

The crust-core transition density in the present work is estimated by adopting the thermodynamical approach under the condition that the energy per nucleon $E(\rho,\delta)$ in nuclear matter at nucleon density ρ and isospin asymmetry $\delta \equiv (\rho_n-\rho_p)/\rho$ is approximated by the isospin-parabolic expansion,

$$E(\rho,\delta) \approx E_0(\rho) + E_{\rm sym}(\rho)\cdot\delta^2. \quad (1)$$

The crust-core transition point is obtained when the uniform matter starts to be separated into a mixture containing single nucleons and clusters. The transition density is specifically calculated by the vanishing effective incompressibility of uniform NS matter under β equilibrium and charge neutrality conditions,

$$K_\mu = \rho^2\frac{d^2E_0}{d\rho^2} + 2\rho\frac{dE_0}{d\rho} + \delta^2\left[\rho^2\frac{d^2E_{\rm sym}}{d\rho^2} + 2\rho\frac{dE_{\rm sym}}{d\rho} - 2E_{\rm sym}^{-1}(\rho\frac{dE_{\rm sym}}{d\rho})^2\right]. \quad (2)$$

That is, one can obtain the transition density ρ_t by solving the equation of $K_\mu = 0$. It is noteworthy to mention that the crust-core transition density can be overestimated when the parabolic approximation (Eq. (1)) is used[8]. As indicated in Fig. 5 of Ref. [8], this overestimation mainly appears in the region where the parameters L and $K_{\rm sym}$ are large, i.e., $L >$ 60 MeV and $K_{\rm sym} >$ -100 MeV. However, after filtered by the NS radius data, the probability that they fall in the abovementioned intervals is very small according to our earlier calculations[17]. Therefore, employing the parabolic approximation will hardly change the present results. Furthermore, It also can reduce the discrepancy between the thermodynamical method used in the present work and other approaches like the dynamical method when these EOS parameters are confronted with the NS radius data.

The transition pressure can be approximately written as[18]

$$P_t \approx \frac{K_0}{9}\frac{\rho_t^2}{\rho_0}\left(\frac{\rho_t}{\rho_0}-1\right) + \rho_t\delta_t\left[\frac{1-\delta_t}{2}E_{\rm sym}(\rho_t) + \left(\rho\frac{dE_{\rm sym}(\rho)}{d\rho}\right)_{\rho_t}\delta_t\right], \quad (3)$$

where δ_t is isospin asymmetry corresponding to ρ_t. E_0 and $E_{\rm sym}$ in Eqs. (1) and (2) are the energy per particle in symmetric nuclear matter (SNM) and the nuclear symmetry energy, respectively. They can be parameterized as

$$E_0(\rho) = E_0(\rho_0) + \frac{K_0}{2}(\frac{\rho-\rho_0}{3\rho_0})^2 + \frac{J_0}{6}(\frac{\rho-\rho_0}{3\rho_0})^3, \quad (4)$$

$$E_{\rm sym}(\rho) = E_{\rm sym}(\rho_0) + L(\frac{\rho-\rho_0}{3\rho_0}) + \frac{K_{\rm sym}}{2}(\frac{\rho-\rho_0}{3\rho_0})^2 + \frac{J_{\rm sym}}{6}(\frac{\rho-\rho_0}{3\rho_0})^3, \quad (5)$$

where $E_0(\rho_0)$=-15.9 MeV is the energy per particle at the saturation density ρ_0 for SNM. $K_0 = 9\rho_0^2[\partial^2E_0(\rho)/\partial\rho^2]|_{\rho=\rho_0}$ and $J_0 = 27\rho_0^3[\partial^3E_0(\rho)/\partial\rho^3]|_{\rho=\rho_0}$ represent the incompressibility and the skewness parameters of SNM at ρ_0, respectively. $E_{\rm sym}(\rho_0)$, $L = 3\rho_0[\partial E_{\rm sym}(\rho)/\partial\rho]|_{\rho=\rho_0}$, $K_{\rm sym} = 9\rho_0^2[\partial^2E_{\rm sym}(\rho)/\partial\rho^2]|_{\rho=\rho_0}$ and $J_{\rm sym} = 27\rho_0^3[\partial^3E_{\rm sym}(\rho)/\partial\rho^3]|_{\rho=\rho_0}$ are, respectively, the magnitude, slope, curvature and skewness of nuclear symmetry energy at ρ_0. According to the systematics of terrestrial nuclear experiments and predictions of various nuclear theories, K_0, $E_{\rm sym}(\rho_0)$, and L have the ranges of 220$\sim$ 260 MeV, 28.5$\sim$ 34.9 MeV and 30$\sim$ 90 MeV[19–23], respectively. While the parameters J_0, $K_{\rm sym}$, and $J_{\rm sym}$ characterizing the nuclear EOS at high densities have the wide ranges of $-800 \le J_0 \le 400$ MeV, $-400 \le K_{\rm sym} \le 100$ MeV, and $-200 \le J_{\rm sym} \le 800$ MeV only from the theoretical predictions[24, 25].

In the framework of the minimum NS model, the non-rotating NS consists of neutrons, protons, electrons, and muons under the β equilibrium and charge neutrality conditions, and the relation between pressure and nucleon density in the core of NSs

$$P(\rho,\delta) = \rho^2\frac{d\epsilon(\rho,\delta)/\rho}{d\rho} \quad (6)$$

is controlled by the energy density $\epsilon(\rho,\delta) = \rho[E(\rho,\delta) + M_N] + \epsilon_l(\rho,\delta)$ with M_N and $\epsilon_l(\rho,\delta)$ being the average nucleon mass and the energy densities for leptons which are calculated by the noninteracting Fermi gas model[26], respectively. δ can be obtained through the charge neutrality condition $\rho_p = \rho_e + \rho_\mu$ and the β-equilibrium condition $\mu_n - \mu_p = \mu_e = \mu_\mu \approx 4\delta E_{\rm sym}(\rho)$, where μ denotes the chemical potential calculated by the expression $\mu_i = \partial\epsilon(\rho,\delta)/\partial\rho_i$ for the ith particle.

One can construct the EOS for the core of NSs in term of the expressions of (4), (5) and (6). Below the crust-core transition density, the NV EOS[27] for the inner crust and the BPS EOS[1] for the outer crust are employed.

B. Neutron skin and nuclear droplet model

The neutron skin thickness of a finite nucleus in the nuclear droplet model(DM) is obtained according to the expression[3, 28]

$$\Delta R_{np} = \sqrt{\frac{3}{5}}\left[t - \frac{e^2Z}{70E_{\rm sym}(\rho_0)} + \frac{5}{2R}\left(b_n^2 - b_p^2\right)\right], \quad (7)$$

where $e^2Z/70E_{\rm sym}(\rho_0)$ is a correction term due to the Coulomb interaction. $R = r_0A^{1/3}$ is the nuclear radius. b_n and b_p denote the surface widths of the neutron and proton density profiles, respectively, and usually $b_n = b_p = 1$ fm is used in the standard DM. The quantity t in Eq. (7) is calculated as[3]

$$t = \frac{2r_0}{3E_{\rm sym}(\rho_0)}L(1 - x\frac{K_{\rm sym}}{2L})xA^{1/3}(\delta - \delta_C) \quad (8)$$

with

$$x = \frac{\rho_0 - \rho_A}{3\rho_0}, \delta_C = \frac{e^2Z}{20E_{\rm sym}(\rho_0)R}. \quad (9)$$

Here $\rho_A = 0.1$ fm^{-3} for the nucleus ^{208}Pb and $\rho_A = 0.08$ fm^{-3} for the nucleus ^{48}Ca.

C. Bayesian inference approach

The Bayesian theorem is expressed as

$$P(\mathcal{M}|D) = CP(D|\mathcal{M})P(\mathcal{M}). \quad (10)$$

Here C is a normalization constant. $P(\mathcal{M}|D)$ stands for the obtained posterior probability distribution function (PDF) of the model $\mathcal{M}$ when the data set D is given. $P(D|\mathcal{M})$ is a likelihood function obtained through confronting the theoretical results from the model $\mathcal{M}$ with the data D, and $P(\mathcal{M})$ is the prior probability of the model $\mathcal{M}$ representing the knowledge on the theoretical parameters of $\mathcal{M}$ before being compared with the data D.

In the present work, we randomly sample the transition density in the range of 0.03 fm $^{-3} \leq \rho_t \leq 0.2$ fm $^{-3}$, and the matched six parameter set can be found by solving the equation of K_μ=0 by using Eq. (2). We adopt two ways to generate the posterior PDF of the transition density. One of them is only based on the observed data of NS radii up to now, and the other is based on both the NS radius data and the data of the neutron-skin thickness. For the first way, we use the matched six parameters to construct the NS EOS in the framework of the minimum NS model as described above and put them in the TOV equation to compute the theoretical values of NS radii. Then we can obtain the likelihood of the transition density or the matched set of parameters by confronting these theoretical values of NS radii with the observed values using the following likelihood function,

$$P(D|\mathcal{M}) = \frac{1}{\sqrt{2\pi}\sigma}\exp[-\frac{(R_{\rm th} - R_{\rm obs})^2}{2\sigma^2}], \quad (11)$$

where $R_{\rm th}$ represents the theoretical values. $R_{\rm obs}$ and σ represent the observed values and its 1σ error bar for NS radii. The NS EOS generated above should satisfy the thermodynamical stability condition ($dP/d\epsilon \geq 0$, P denotes the pressure inside NSs) and the causality condition ($0 \leq v_s^2 \leq c^2$, v_s and c denote the speed of sound and light, respectively) at all densities, and should be stiff enough to support the maximum mass of the NS observed up to now. A sharp cut-off at 1.97 M$_\odot$ is used in the present analysis.

For the second way, after obtaining the matched six parameter set using Eq. (2) through sampling the transition density, we let them as the input into the DM to calculate the theoretical values of the neutron skin thickness for ^{208}Pb and ^{48}Ca. Then we can discard these parameter sets and the transition densities when the calculated values for the neutron skin thickness are far from the experimental values using the likelihood function

$$P(D|\mathcal{M}) = \frac{1}{\sqrt{2\pi}\sigma'}\exp[-\frac{(\Delta R_{np}^{\rm th} - \Delta R_{np}^{\rm exp})^2}{2\sigma'^2}], \quad (12)$$

where $\Delta R_{np}^{\rm th}$ and $\Delta R_{np}^{\rm exp}$ are respectively the theoretical and experimental values, and σ' represent the 1σ error bar for the experimental data. After this, the rest of the parameter sets will be used to construct the NS EOS and calculate the posterior PDFs of the transition density as described above.

The observed data for the NS radii and the experimental data for the neutron-skin thickness used in this work are summarized in Table I. These NS data include: (i) $R_{1.4} = 11.9^{+1.4}_{-1.4}$ km at 90% confidence level (CFL) by analyzing the GW170817 source reported by the LIGO/Virgo Collaboration[29]; (ii) $R_{1.4} = 10.8^{+2.1}_{-1.6}$ km at 90% CFL by analyzing the same source of GW170817[30]; (iii) $R_{1.4} = 11.7^{+1.1}_{-1.1}$ km at 90% CFL reported earlier by analyzing the quiescent low-mass X-ray binaries (QLMXBs)[31]; (iv) Reported by the NICER Collaboration[33, 36] at 68% CFL, $R = 12.71^{+1.14}_{-1.19}$ with mass of $1.34^{+0.15}_{-0.16}$M$_\odot$[32] and $R = 13.02^{+1.24}_{-1.06}$ with mass of $1.44^{+0.15}_{-0.14}$M$_\odot$[36] for the source of PSR J0030+0451, $R = 13.7^{+2.6}_{-1.5}$ with mass of $2.08^{+0.07}_{-0.07}$M$_\odot$ for the source of PSR J0740+6620. The data for the neutron-skin thickness are $\Delta R_{np} = 0.121^{+0.026}_{-0.026}$ fm and $\Delta R_{np} = 0.283^{+0.071}_{-0.071}$ fm for ^{48}Ca and ^{208}Pb, respectively, which taken from Refs. [34, 35] recently reported by the CREX and PREX-2 Collaborations.

The Metropolis-Hastings algorithm within a Markov-Chain Monte Carlo (MCMC) approach is adopted to generate the posterior PDFs of the model parameters. Not only the PDFs of the individual parameters but the PDFs for the two-parameter correlations can be calculated by integrating over all other parameters using the marginal estimation approach. The initial samples in the so-called burn-in period are thrown away[37] so that the MCMC process can start from an equilibrium distribution. The 40,000 steps for burn-in progress and the rest one million steps for calculating the PDF of the transition density are taken in the present analysis.

TABLE I: Data for the NS radius and the neutron-skin thickness used in the present work.

Mass($M_\odot$)	Radius R (km)	Source and Reference
1.4	$11.9^{+1.4}_{-1.4}$(90% CFL)	GW170817 [29]
1.4	$10.8^{+2.1}_{-1.6}$ (90% CFL)	GW170817 [30]
1.4	$11.7^{+1.1}_{-1.1}$ (90% CFL)	QLMXBs [31]
$1.34^{+0.15}_{-0.16}$	$12.71^{+1.14}_{-1.19}$ (68% CFL)	PSR J0030+0451 [32]
$1.44^{+0.15}_{-0.14}$	$13.0^{+1.2}_{-1.0}$ (68% CFL)	PSR J0030+0451 [33]
$2.08^{+0.07}_{-0.07}$	$13.7^{+2.6}_{-1.5}$ (68% CFL)	PSR J0740+6620 [33]
Nucleus	ΔR_{np} (fm)	Source and Reference
^{48}Ca	$0.121^{+0.026}_{-0.026}$(68% CFL)	CREX[34]
^{208}Pb	$0.283^{+0.071}_{-0.071}$(68% CFL)	PREX-2[35]

III. RESULTS AND DISCUSSIONS

A. Exploring the crust-core transition density via the NS observations

The posterior PDFs of the crust-core transition density ρ_t and the corresponding transition pressure P_t as well as their correlations with the EOS coefficients are plotted in Fig. 1. In the calculations, the two types of prior for ρ_t are adopted. The first form is the uniform distribution which is a better choice as we have no idea about ρ_t, and this case is displayed in Fig. 1 by the black curves. The second form is the Gaussian distribution with a average value of 0.078 fm^{-3} and a standard deviation of 0.04 as used in Ref. [3], which is indicated by the purple curve in Fig. 1. In the panels located in the upper two rows we show the posterior PDFs of the correlations mentioned above using the uniform priors for ρ_t, and these panels in the bottom two rows show the results using the Gaussian priors. These results are only based on the observed data of NS radii summarized in Table I.

A two-humped posterior distribution for ρ_t is observed for both the uniform and Gaussian priors used in the calculations. The first peak is located at $\rho_t = 0.08$ fm^{-3} which is often used as its fiducial value in the literature, and the second peak is at $\rho_t = 0.1$ fm^{-3}. The calculated 68% and 90% credible intervals by using the highest posterior density interval approach for ρ_t and P_t are listed in Table II. We can see that, relative to the prior distributions, the posterior PDFs of ρ_t are narrowed down to the small intervals, which reflects the fact that the crust-core transition density is sensitive to the NS radius. It has a larger probability to fall in the region where ρ_t has values larger than 0.1 fm^{-3} when a uninformative prior is used. This can be attributed to the correlations between ρ_t and some EOS parameters and will be discussed later.

A better constraint on ρ_t is found when the Gaussian prior is used in comparison with these using the uniform prior. This is easy to understand that more information is available for the Gaussian prior than these results from the uniform prior before confronting them with the NS radius data. The generated ranges of P_t, i.e., $0.05^{+1.25}_{-0.04}$ MeV/fm^3 using the uniform prior and $0.1^{+0.28}_{-0.1}$ MeV/fm^3 using the Gaussian prior at 68% confidence level as listed in Table II, can cover these calculated by using the meta-modelling, dynamical and thermodynamical models, see the Table I in Ref. [15], however, the most probable values are smaller than them. Our results for ρ_t are consistent with these in the literature.

Let's turn to explore the correlations among ρ_t, P_t and the EOS parameters. Here we do not concern the correlations among the EOS parameters which are consistent with these reported in our earlier publications[17, 40]. The low-order parameters such as $E_{\rm sym}(\rho_0)$ and K_0 are hardly correlated with the transition. However, as mentioned in Ref. [12], the condition $K_\mu = 0$ requires a larger ρ_t as K_0 increases. This phenomenon is displayed in Fig. 1, namely a weak positive correlation is found between ρ_t and K_0 for the cases using both the uniform and Gaussian priors.

Consistent with the results reported in Ref. [16], the strong correlations among ρ_t and the isovector compressibility $K_{\rm sym}$, skewness $J_{\rm sym}$ are discovered. A negatively correlation between ρ_t and $K_{\rm sym}$ is inconsistent with the results in Ref. [16], in which the EOS parameters are filtered by the predictions from the effective field theory and surface coefficients are determined by the nuclear masses in the framework of extended Thomas Fermi approximation method. The positively correlations between ρ_t and $J_{\rm sym}$, and ρ_t and P_t showed in Fig. 1 are in agreement with these in Ref. [15, 16]. The transition is not affected by the skewness of symmetric nuclear matter J_0.

L shows a negatively correlation with ρ_t. Interestingly, a positively correlation appears in the region at $\rho_t > 0.1$ fm^{-3} for the case using the uniform prior. This does not happen for the case using the Gaussian prior. Do this relate to the the shoulder indicated in posterior PDF of ρ_t using the uniform prior in Fig. 1 ? To answer this question, we plot the L-$K_{\rm sym}$ correlations from three types of calculations as indicated in Fig. 2, i.e., using the uniform and Gaussian priors based on the NS radius data, using

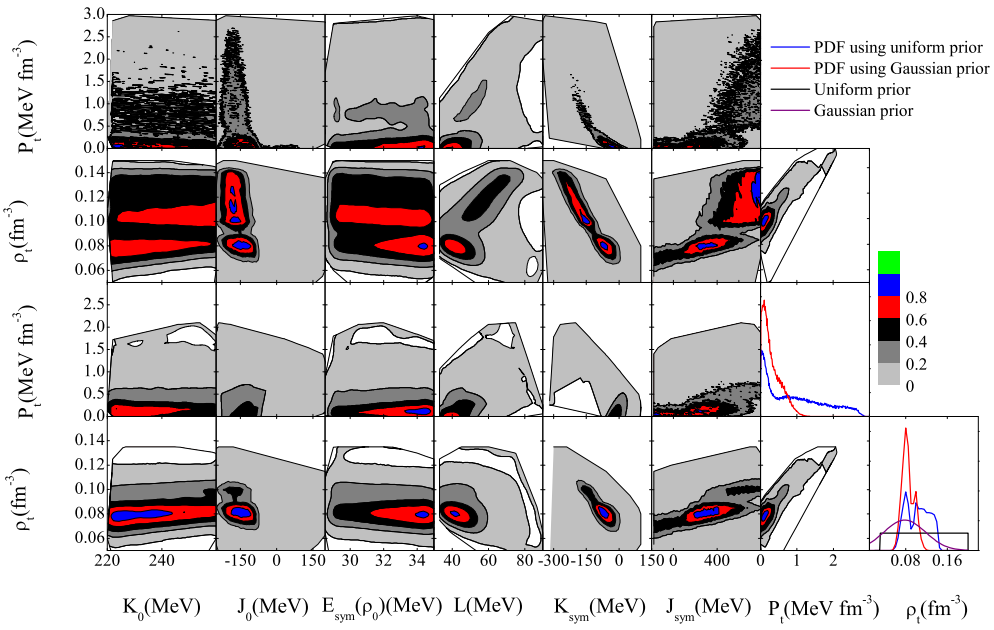

FIG. 1: (color online)Posterior probability distribution functions of the crust-core transition density and pressure as well as their correlations with the EOS parameters. The calculations are performed by adopting the uniform (shown by blue curves) and Gaussian (shown by red curves) priors for the transition density based on the NS radius data. For comparison, the uniform (shown by black curve) and Gaussian (shown by purple curve) forms for the prior distributions of the transition density are included. The correlations in the upper (bottom) two rows are calculated by using the uniform (Gaussian) prior for the transition density.

TABLE II: Most probable values and the 68% and 90% credible intervals of ρ_t and P_t calculated by using the uniform prior, the Gaussian prior, the neutron-star plus neutron-skin thickness data (NS+NST), the $L-K_{\rm sym}$ correlation in Ref. [38] by Holt et al., the $L-K_{\rm sym}$ correlation in Ref. [39] by Mondal et al., the $L-K_{\rm sym}$ correlation in Ref. [24] by Tews et al..

	Uniform prior	Gaussian prior	NS+NST	Holt et al.(2018)	Mondal et al.(2017)	Tews et al. (2017)
ρ_t	$0.08^{+0.06}_{-0.005}$,$0.08^{+0.06}_{-0.025}$	$0.08^{+0.01}_{-0.03}$,$0.08^{+0.025}_{-0.03}$	$0.075^{+0.005}_{-0.01}$,$0.075^{+0.025}_{-0.01}$	$0.08^{+0.005}_{-0.005}$,$0.08^{+0.01}_{-0.015}$	$0.1^{+0.005}_{-0.01}$,$0.1^{+0.01}_{-0.02}$	$0.1^{+0.005}_{-0.01}$,$0.1^{+0.01}_{-0.02}$
P_t	$0.05^{+1.25}_{-0.04}$,$0.05^{+2.13}_{-0.04}$	$0.1^{+0.28}_{-0.1}$,$0.1^{+0.6}_{-0.1}$	$0.1^{+0.2}_{-0.08}$,$0.1^{+0.64}_{-0.08}$	$0.16^{+0.01}_{-0.06}$,$0.16^{+0.18}_{-0.08}$	$0.6^{+0.18}_{-0.14}$,$0.6^{+0.28}_{-0.28}$	$0.6^{+0.18}_{-0.14}$,$0.6^{+0.28}_{-0.26}$

the uniform prior based on both the NS radius and neutron skin thickness data. There are two phenomena in Fig. 2 we can see. One is the anti-correlations shown in left and right panels, and highly weak correlation shown in the middle panel between L and $K_{\rm sym}$, and the other is, as shown in the left panel in Fig. 2, $K_{\rm sym}$ has a high probability to stay in the region where $K_{\rm sym}$ is extremely negative, i.e. $K_{\rm sym}$ < -200 MeV. The latter is obviously responsible for the shoulder because the shoulder for the posterior PDF of ρ_t disappears as shown in Fig. 3 though the L-$K_{\rm sym}$ anti-correlations are same in their calculations in the left and right panels. Therefore, $K_{\rm sym}$ plays a more important role in constraining the crust-core transition density of NSs than the L-$K_{\rm sym}$ correlation as studied in Ref. [12]. The transition pressure are weakly correlated to the EOS parameters.

B. Effect of neutron-skin thickness and comparison with other calculations

It has been known that the neutron-skin thickness is a effective probe to the nuclear symmetry energy, especially its slope parameter[41, 42]. The latter plays an important role in determining the crust-core transition density of NSs. Shown in Fig. 3 are the results same as these in Fig. 1 but based on not only the NS radius data but also the neutron-skin thickness data. In the calculations, we first perform a Bayesian inference of the coefficients $E_{\rm sym}(\rho_0)$, L and $K_{\rm sym}$ in the framework of the nucle-

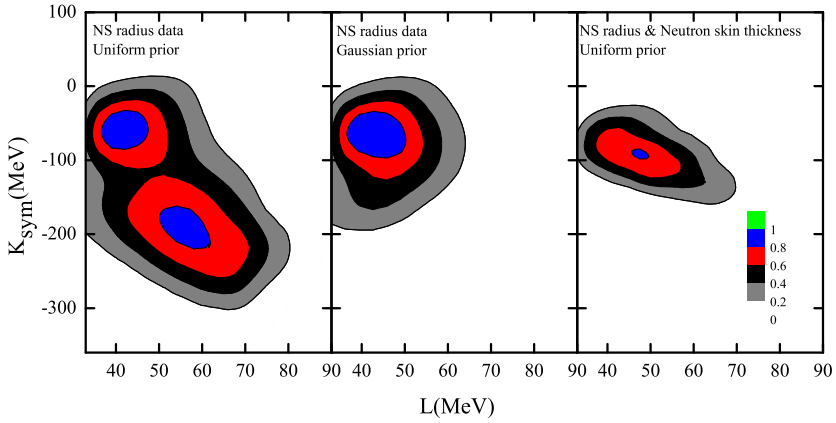

FIG. 2: (color online)Correlations between L and $K_{\rm sym}$ calculated from the NS radius data by using the uniform (Left) and Gaussian (Middle) priors, and from both the neutron-star radius and neutron-skin thickness data (Right) by using the uniform prior.

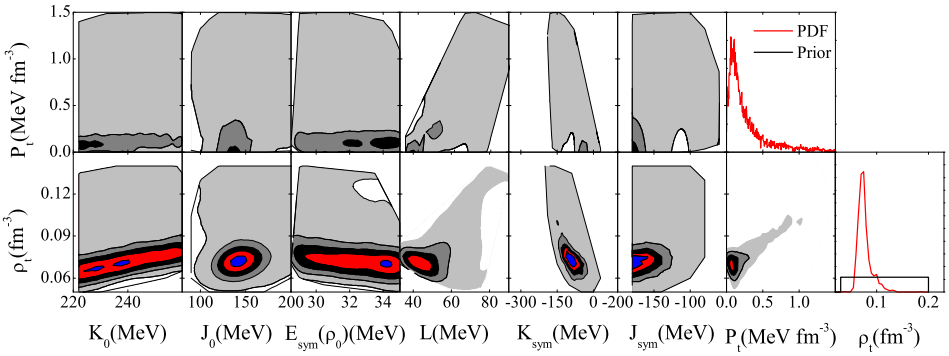

FIG. 3: (color online)Posterior probability distribution functions of the crust-core transition density and pressure as well as their correlations with the EOS parameters. In the calculations, both the neutron-skin thickness and NS radius data are adopted. The prior distribution (shown by black curve) for the transition density is included.

ar droplet model as described in Sec. II B based on the neutron-skin thickness data reported by the CREX[34] and PREX-2[35] Collaborations as listed in Table I. After that, we regard the obtained distributions of these parameters and the matched transition density as their priors to infer the posterior PDF of the transition density based on the NS radius data within the minimum NS model. It is worth noting that there exists significant controversy about constraining the slope of the symmetry energy through the neutron-skin thickness data of ^{48}Ca and ^{208}Pb reported by the CREX and PREX-2 Collaborations. A recent study demonstrates that the ranges for the slope L obtained from the CREX and the PREX-2 are completely inconsistent[43]. More accurate measurements are needed. Fortunately, there are many methods to determine the neutron-skin thickness, i. e., the configurational information entropy analysis[44, 45].

As seen in Fig. 3, the correlations are roughly same as these in Fig. 1. A weak anti-correlation between the symmetry energy magnitude $E_{\rm sym}(\rho_0)$ and ρ_t is observed due to the constraint from the neutron-skin thickness data on $E_{\rm sym}(\rho_0)$. The range for $K_{\rm sym}$ is smaller than these using only the NS radius data, which is also because of the effect of the neutron-skin thickness data. The constraint on ρ_t obtained is improved in comparison with these only based on the NS data as listed in Table II. This is because the parameters L and $K_{\rm sym}$ are better constrained when the neutron-skin thickness data are taken into consideration.

In Fig. 4 we compare our results with these inferred using a compressible liquid-drop model within a Bayesian framework[15], in which there are two filters, i.e., the low density (LD) behavior of the energy functionals that should be rigorously limited in the uncertainty intervals of the effective field theory calculation for symmetric and pure neutron matter in Ref. [46] and the high den-

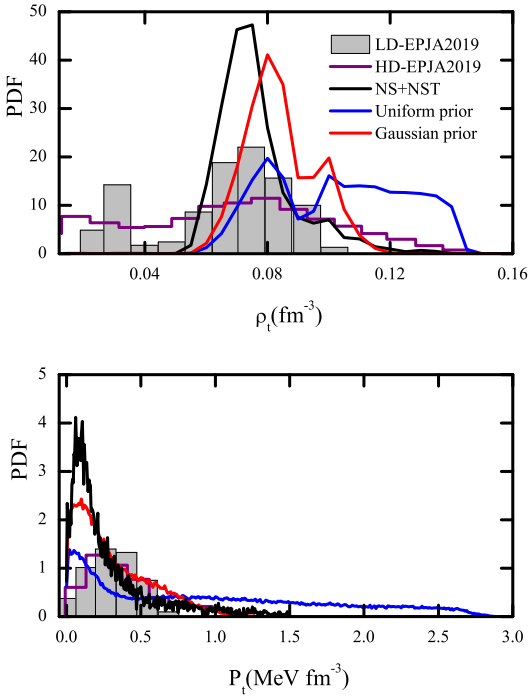

FIG. 4: (color online)Posterior probability distribution functions of the crust-core transition density and pressure based on only the NS radius data by using the uniform (shown by blue curve) and Gaussian (shown by red curve) priors, and based on both the NS radius and neutron-skin thickness data by using the uniform prior indicated by NS+NST (shown by black curve). For comparison, the results in Ref. [15] shown by LD-EPJA2019 and HD-EPJA2019 are included.

sity (HD) behavior of the functionals that should obey the conditions such as positive symmetry energy at all densities, causality and so on[15]. One can see that our results overlap with theirs. There is a long tail for P_t for the case using the uniform prior in the calculations, which is because the large probability of ρ_t exists in the region at $\rho_t > 0.1$ fm^{-3}. Our most probable values for P_t are smaller than these from Ref. [15].

C. Effect of L-$K_{\rm sym}$ correlations

It has been reported that L-$K_{\rm sym}$ correlations have a significant impact on both the crust-core transition density and pressure[12]. To further explore this effect, we take three typical L-$K_{\rm sym}$ correlations predicted in the literature as the priors to infer the posterior PDF of ρ_t. For completeness and ease of discussions, here we describe briefly the three correlations. The first one is based on the theoretical predictions from 240 Skyrme Hartree-Fock and 263 relativistic mean-field calculations[39] by

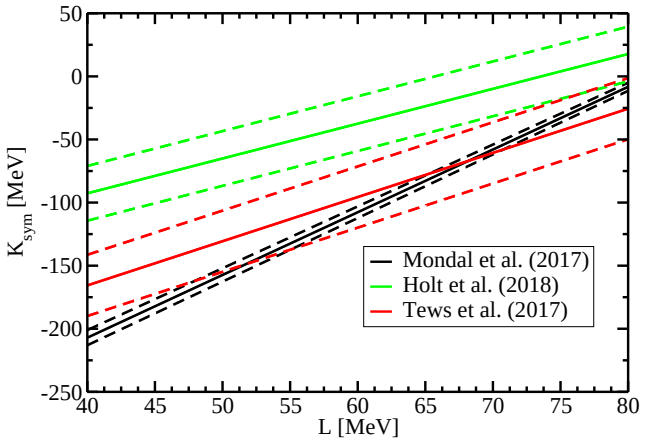

FIG. 5: (Color online) $L - K_{\rm sym}$ correlations from Tews *et al.* [24] (shown by red curves), Mondal *et al.* [39] (shown by black curves) and Holt *et al.* [38] (shown by green curves). The solid and dashed lines respectively denote the means and the boundaries of each correlation. Taken from Ref. [12].

Mondal *et al.* and written as

$$K_{\rm sym} = (-4.97\pm0.07)(3E_{\rm sym}(\rho_0)-L)+66.80\pm2.14\ {\rm MeV}. \quad (13)$$

The second one is taken from Ref. [24] by Tews *et al.* and written as

$$K_{\rm sym} = 3.50L - 305.67 \pm 24.26\ {\rm MeV}. \quad (14)$$

In the framework of the Fermi liquid theory, Holt and Lim[38] derived the expressions $L = 6.70E_{\rm sym}(\rho_0) - 148.60\pm4.37$ MeV and $K_{\rm sym} = 18.50E_{\rm sym}(\rho_0) - 613.18 \pm 9.62$ MeV. Thus one can formulate the last relation between L and $K_{\rm sym}$ as[12]

$$K_{\rm sym} = 2.76L - 203.07 \pm 21.69\ {\rm MeV}. \quad (15)$$

These correlations are shown in Fig. 5. The discrepancy among the correlations by Mondal *et al.* and Tews *et al.* is not too much larger because they are from the same sets of theory predictions. However, These depicted in Figs. 2 and 5 are highly different. This illustrates that the L-$K_{\rm sym}$ correlations are strongly model dependent and constraining them has a long way to go.

In the Bayesian inference approach, after considering the abovementioned correlations, L and $K_{\rm sym}$ will not be independent when we randomly sample them between their specific ranges. In the calculations performed in this subsection, the uniform prior for ρ_t and only the NS radius data are employed. The generated posterior PDFs for ρ_t and P_t are represented in Fig. 6, and the corresponding confidence intervals are summarized in Table II. One can see that, as stated in Ref. [12], the $L - K_{\rm sym}$ correlations play a significant role in constraining both

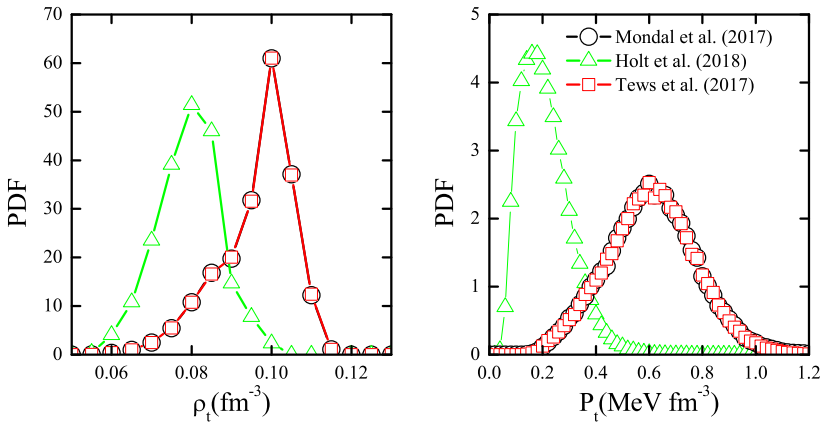

FIG. 6: (color online)Posterior probability distribution functions of the crust-core transition density and pressure as the three correlations of $L - K_{\rm sym}$ as in Fig. 5 are used in the calculations.

the transition density and pressure. There are at least two observations we can obtain: (i)The results from the relations by Mondal *et al.* and Tews *et al.* are completely consistent. This is mainly because this two correlations largely overlap within the allowed error limits; (ii)The most probable values from the relations by Holt *et al.* are highly different from the other two cases. For the latter, the transition density and pressure have the larger values than these for the former. This is due to the fact that $K_{\rm sym}$ is not extremely negative in the relation by Holt *et al.*, i.e. $K_{\rm sym}$ having the values higher than about -115 MeV as shown by green curves in Fig. 5. The present results are consistent with these in Ref. [12], in which the authors studied the effects of $L - K_{\rm sym}$ correlations on the crust-core transition density and pressure by adopting the fixed values of the other parameters in Eqs. (4) and (5).

IV. SUMMARY

In summary, using the thermodynamical approach to calculate the crust-core transition density and an explicitly isospin-dependent parametric EOS for the core of NSs within the minimum NS model, the Bayesian inference of the crust-core transition density based on the NS radius and neutron-skin thickness data is performed. The uniform and Gaussian forms for prior distributions of transition density are employed in the calculations. It is found that the transition density has a larger probability to take the values larger than 0.1 fm^{-3} when the uniform prior is used, which does not happen as the Gaussian prior is used. To take the values smaller than -200 MeV for $K_{\rm sym}$ is responsible for this phenomenon.

The negatively (positively) correlations between ρ_t and L and between ρ_t and $K_{\rm sym}$ (between ρ_t and K_0, between ρ_t and $J_{\rm sym}$ and between ρ_t and P_t) are observed. Based on the NS radius data reported so far, the generated 68% confidence intervals for ρ_t are respectively $0.08^{+0.06}_{-0.005}$ fm^{-3} and $0.08^{+0.01}_{-0.03}$ fm^{-3} when the uniform and Gaussian priors are adopted. When the EOS parameters are first filtered by the neutron-skin thickness data, the obtained one is $0.075^{+0.005}_{-0.01}$ fm^{-3}. We also check the impact of L-$K_{\rm sym}$ correlations on the posterior PDFs of ρ_t and P_t. The results from the L-$K_{\rm sym}$ relations reported by Tews *et al.* [24] and Mondal *et al.*[39] are completely overlapped, and the results reported from Holt *et al.* [38] are smaller than these from the other two L-$K_{\rm sym}$ relations.

Acknowledgement: This work is supported by the Shanxi Provincial Foundation for Returned Overseas Scholars under Grant No 20220037, the Natural Science Foundation of Shanxi Province under Grant No 20210302123085, and the discipline construction project of Yuncheng university.

[1] G. Baym, C. Pethick, P. Sutherland, The ground state of matter at high densities: equation of state and stellar models. The Astrophys. J. **170**, 299 (1971). doi:10.1086/151216

[2] N. Paar, C.C. Moustakidis, T. Marketin, et al., Neutron star structure and collective excitations of finite nuclei. Phys. Rev. C **90**, 011304 (2014). doi:10.1103/PhysRevC.90.011304

[3] M. Centelles, X. Roca-Maza, X. Vinas, et al., Nuclear symmetry energy probed by neutron skin thickness of nuclei. Phys. review letters **102**, 122502 (2009). doi:10.1103/PhysRevLett.102.122502

[4] C. Horowitz, J. Piekarewicz, Neutron star structure and the neutron radius of p 208 b. Phys. Rev. Lett. **86**, 5647 (2001). doi:10.1103/PhysRevLett.86.5647

[5] L. Tsaloukidis, C. Margaritis, C.C. Moustakidis, Effects of the equation of state on the core-crust interface of slowly rotating neutron stars. Phys. Rev. C **99**, 015803 (2019). doi:10.1103/PhysRevC.99.015803

[6] J. Fang, H. Pais, S. Pratapsi, et al., Crust-core transition of a neutron star: Effects of the symmetry energy and temperature under strong magnetic fields. Phys. Rev. C **95**, 062801 (2017). doi:10.1103/PhysRevC.95.062801

[7] C. Gonzalez-Boquera, M. Centelles, X. Viñas, et al., Core-crust transition in neutron stars with finite-range interactions: The dynamical method. Phys. Rev. C **100**, 015806 (2019). doi:10.1103/PhysRevC.100.015806

[8] J. Xu, L.W. Chen, B.A. Li, et al., Nuclear constraints on properties of neutron star crusts. The Astrophys. J. **697**, 1549 (2009). doi:10.1088/0004-637X/697/2/1549

[9] J.M. Lattimer, Y. Lim, Constraining the symmetry parameters of the nuclear interaction. The Astrophys. J. **771**, 51 (2013). doi:10.1088/0004-637X/771/1/51

[10] S.S. Bao, H. Shen, Impact of the symmetry energy on nuclear pasta phases and crust-core transition in neutron stars. Phys. Rev. C **91**, 015807 (2015). doi:10.1103/PhysRevC.91.015807

[11] C.C. Moustakidis, Effect of the symmetry energy on the location of the inner edge of the neutron star crust. Phys. Rev. C **86**, 015801 (2012). doi:10.1103/PhysRevC.86.015801

[12] B.A. Li, M. Magno, Curvature-slope correlation of nuclear symmetry energy and its imprints on the crust-core transition, radius, and tidal deformability of canonical neutron stars. Phys. Rev. C **102**, 045807 (2020). doi:10.1103/PhysRevC.102.045807

[13] Z.W. Liu, Z. Qian, R.Y. Xing, et al., Nuclear fourth-order symmetry energy and its effects on neutron star properties in the relativistic hartree-fock theory. Phys. Rev. C **97**, 025801 (2018). doi:10.1103/PhysRevC.97.025801

[14] H. Pais, A. Sulaksono, B.K. Agrawal, et al., Correlation of the neutron star crust-core properties with the slope of the symmetry energy and the lead skin thickness. Phys. Rev. C **93**, 045802 (2016). doi:10.1103/PhysRevC.93.045802

[15] T. Carreau, F. Gulminelli, J. Margueron, Bayesian analysis of the crust-core transition with a compressible liquid-drop model. The Eur. Phys. J. A **55**, 188 (2019). doi:https://doi.org/10.1140/epja/i2019-12884-1

[16] S. Antić, D. Chatterjee, T. Carreau, et al., Quantifying the uncertainties on spinodal instability for stellar matter through meta-modeling. J. Phys. G: Nucl. Part. Phys. **46**, 065109 (2019). doi:10.1088/1361-6471/ab1a51

[17] W.J. Xie, B.A. Li, Bayesian inference of high-density nuclear symmetry energy from radii of canonical neutron stars. The Astrophys. J. **883**, 174 (2019). doi:10.3847/1538-4357/ab3f37

[18] J.M. Lattimer, M. Prakash, Neutron star observations: Prognosis for equation of state constraints. Phys. reports **442**, 109–165 (2007). doi:https://doi.org/10.1016/j.physrep.2007.02.003

[19] P. Danielewicz, R. Lacey, W.G. Lynch, Determination of the equation of state of dense matter. Sci. **298**, 1592–1596 (2002). doi:10.1126/science.1078070

[20] S. Shlomo, V. Kolomietz, G. Colo, Deducing the nuclear-matter incompressibility coefficient from data on isoscalar compression modes. The Eur. Phys. J. A-Hadrons Nucl. **30**, 23–30 (2006). doi:https://doi.org/10.1140/epja/i2006-10100-3

[21] J. Piekarewicz, Do we understand the incompressibility of neutron-rich matter? J. Phys. G: Nucl. Part. Phys. **37**, 064038 (2010). doi:10.1088/0954-3899/37/6/064038

[22] B.A. Li, X. Han, Constraining the neutron–proton effective mass splitting using empirical constraints on the density dependence of nuclear symmetry energy around normal density. Phys. Lett. B **727**, 276–281 (2013). doi:https://doi.org/10.1016/j.physletb.2013.10.006

[23] M. Oertel, M. Hempel, T. Klähn, et al., Equations of state for supernovae and compact stars. Rev. Mod. Phys. **89**, 015007 (2017). doi:10.1103/RevModPhys.89.015007

[24] I. Tews, J.M. Lattimer, A. Ohnishi, et al., Symmetry parameter constraints from a lower bound on neutron-matter energy. The Astrophys. J. **848**, 105 (2017). doi:10.3847/1538-4357/aa8db9

[25] N.B. Zhang, B.J. Cai, B.A. Li, et al., How tightly is the nuclear symmetry energy constrained by a unitary fermi gas? Nucl. Sci. Tech. **28**, 1–7 (2017). doi:https://doi.org/10.1007/s41365-017-0336-2

[26] N.B. Zhang, B.A. Li, J. Xu, Combined constraints on the equation of state of dense neutron-rich matter from terrestrial nuclear experiments and observations of neutron stars. The Astrophys. J. **859**, 90 (2018). doi:10.3847/1538-4357/aac027

[27] J.W. Negele, D. Vautherin, Neutron star matter at sub-nuclear densities. Nucl. Phys. A **207**, 298–320 (1973). doi:https://doi.org/10.1016/0375-9474(73)90349-7

[28] M. Warda, X. Vinas, X. Roca-Maza, et al., Neutron skin thickness in the droplet model with surface width dependence: Indications of softness of the nuclear symmetry energy. Phys. Rev. C **80**, 024316 (2009). doi:10.1103/PhysRevC.80.024316

[29] B.P. Abbott, R. Abbott, T. Abbott, et al., Gw170817: Measurements of neutron star radii and equation of state. Phys. review letters **121**, 161101 (2018). doi:10.1103/PhysRevLett.121.161101

[30] S. De, D. Finstad, J.M. Lattimer, et al., Tidal deformabilities and radii of neutron stars from the observation of gw170817. Phys. review letters **121**, 091102 (2018). doi:10.1103/PhysRevLett.121.091102

[31] J.M. Lattimer, A.W. Steiner, Constraints on the symmetry energy using the mass-radius relation of neutron stars. The Eur. Phys. J. A **50**, 1–24 (2014). doi:https://doi.org/10.1140/epja/i2014-14040-y

[32] T.E. Riley, A.L. Watts, S. Bogdanov, et al., A nicer view of psr j0030+ 0451: millisecond pulsar parameter estimation. The Astrophys. J. Lett. **887**, L21 (2019). doi:10.3847/2041-8213/ab481c

[33] E. Fonseca, H.T. Cromartie, T.T. Pennucci, et al., Refined mass and geometric measurements of the high-mass psr j0740+ 6620. The Astrophys. J. Lett. **915**, L12 (2021). doi:10.3847/2041-8213/ac03b8

[34] D. Adhikari, H. Albataineh, D. Androic, et al., Precision determination of the neutral weak form factor of ca 48. Phys. Rev. Lett. **129**, 042501 (2022). doi:10.1103/PhysRevLett.129.042501

[35] D. Adhikari, H. Albataineh, D. Androic, et al., Accurate determination of the neutron skin thickness of pb 208 through parity-violation in electron scattering. Phys. review letters **126**, 172502 (2021). doi:10.1103/PhysRevLett.126.172502

[36] M.C. Miller, F. Lamb, A. Dittmann, et al., The radius of psr j0740+ 6620 from nicer and xmm-newton data. The Astrophys. J. Lett. **918**, L28 (2021). doi:10.3847/2041-8213/ac089b
[37] R. Trotta, Bayesian methods in cosmology. arXiv preprint arXiv:1701.01467 . doi:https://doi.org/10.48550/arXiv.1701.01467
[38] J.W. Holt, Y. Lim, Universal correlations in the nuclear symmetry energy, slope parameter, and curvature. Phys. Lett. B **784**, 77–81 (2018). doi:https://doi.org/10.1016/j.physletb.2018.07.038
[39] C. Mondal, B. Agrawal, J. De, et al., Interdependence of different symmetry energy elements. Phys. Rev. C **96**, 021302 (2017).
[40] W.J. Xie, B.A. Li, Bayesian inference of the symmetry energy of superdense neutron-rich matter from future radius measurements of massive neutron stars. The Astrophys. J. **899**, 4 (2020). doi:10.3847/1538-4357/aba271
[41] J. Xu, Constraining isovector nuclear interactions with giant dipole resonance and neutron skin in 208pb from a bayesian approach. Chin. Phys. Lett. **38**, 042101 (2021). doi:10.1088/0256-307X/38/4/042101
[42] J. Xu, W.J. Xie, B.A. Li, Bayesian inference of nuclear symmetry energy from measured and imagined neutron skin thickness in sn 116, 118, 120, 122, 124, 130, 132, pb 208, and ca 48. Phys. Rev. C **102**, 044316 (2020). doi:10.1103/PhysRevC.102.044316
[43] S. Tagami, T. Wakasa, M. Yahiro, Slope parameters determined from crex and prex2. Results Phys. **43**, 106037 (2022). doi:https://doi.org/10.1016/j.rinp.2022.106037
[44] H.L. Wei, X. Zhu, C. Yuan, Configurational information entropy analysis of fragment mass cross distributions to determine the neutron skin thickness of projectile nuclei. Nucl. Sci. Tech. **33**, 111 (2022). doi:https://doi.org/10.1007/s41365-022-01096-w
[45] C.W. Ma, Y.P. Liu, H.L. Wei, et al., Determination of neutron-skin thickness using configurational information entropy. Nucl. Sci. Tech. **33**, 6 (2022). doi:https://doi.org/10.1007/s41365-022-00997-0
[46] C. Drischler, K. Hebeler, A. Schwenk, Asymmetric nuclear matter based on chiral two- and three-nucleon interactions. Phys. Rev. C **93**, 054314 (2016). doi:10.1103/PhysRevC.93.054314